ACCOUNTS of chemical research

Article

Cite This: Acc. Chem. Res. 2019, 52, 780−790

pubs.acs.org/accounts

Phase Control in Inorganic Nanocrystals through Finely Tuned Growth at an Ultrathin Scale

Haoyi Li and Xun Wang*

Key Lab of Organic Optoelectronics and Molecular Engineering, Department of Chemistry, Tsinghua University, Beijing 100084, China

CONSPECTUS: Crystalline polymorphs have been considered a prevailing phenomenon in inorganic nanocrystals and provide approaches to modulate fundamental properties and innovative advanced applications. As a basic demand for phase engineering, accessible and controllable synthetic methodologies are indispensable for acquisition of high-quality products in expected phases. Phase stability is also a non-negligible issue that determines continuous gains of functionality and long-term sustainability of characteristic features. Maintaining structural stability of metastable phases provides challenges and opportunities for investigations on fascinating properties and intriguing applications of inorganic nanocrystals. Phase engineering is of great significance to acquire metallic (1T) and semiconducting (2H) Mo- and W-based dichalcogenides for hydrogen evolution reaction (HER) and CO_2 reduction reaction (CO_2RR), respectively. The catalysts in 1T phase have superior electron transfer kinetics and abundant active sites on both basal planes and edges for HER, while ones in 2H phase are preferentially deployed for CO_2RR to utilize edge sites for catalysis and restrain competitive HER activity. In addition, the photocatalytic performance for HER has been enhanced by combining anatase and rutile phases because electron transfer between the two phases during photocatalysis facilitates the separation of charge carriers and thus impedes the recombination of electron−hole pairs. Although ample effort has been devoted to developing phase engineering, principle understanding at an ultrathin scale remains obscure.

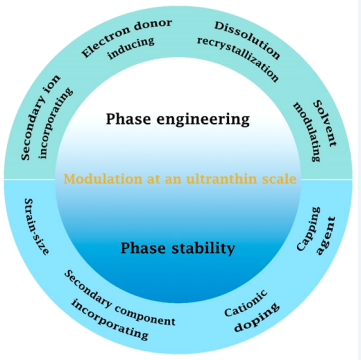

In this Account, we provide comprehensive insight into work from our group regarding controllable synthesis of inorganic nanocrystals with phase engineering, critical effects on phase stability, and noteworthy studies on phase-related properties and applications. For bulk materials, phase control and transition have a large energy barrier, so they can only be achieved under rigorous conditions. However, at the initial stage of synthesis, especially for nucleation, there are a small quantity of chemical bonds that contribute to regulate phase and structure with ease. In our work, we mainly modulate nucleation and growth at an ultrathin scale to demonstrate facile approaches for phase engineering. This unique perspective makes for a distinct guidance of controllable synthesis and deliberate stabilization of inorganic nanomaterials with phase engineering.

We have developed a series of synthetic strategies for phase engineering to fabricate inorganic nanocrystals in a specific phase with controlled size and composition and adjustable morphologies and surface features. Four sorts of models (MoS_2, ZrO_2, In_2O_3, and TiO_2) are used for demonstrating finely tuned growth at an ultrathin scale. However, phase engineering has been regarded as immature because only one phase in polymorphs is thermodynamically stable generally. Phase stability of metastable nanocrystals has attracted much interest. Our substantial investigations illustrate several crucial factors on phase stability, leading to inspiration for facilitating persistent emergence of characteristics and functionalities.

By full use of the features of a specific phase, we spotlight ligand-induced surface interactions on coverage-dependent electronic structures and chemisorption effects at one-unit thickness of TiO_2(B) nanomaterials with phase engineering. Meanwhile, an energy conversion system for overall water splitting (OWS) drives forward steps in function-oriented synthesis of MoS_2-based nanomaterials with phase engineering. In the last section, we summarize this theme and highlight several promising directions for future development.

1. INTRODUCTION

Achievements in comprehensive understanding of scientific fundamentals of inorganic nanocrystals have been facilitated since the concept and features of phase were recognized and explored.[1−5] A phase is a substance with identical properties of physics and chemistry. One phase corresponds to one crystal structure for a category of materials that generally has diverse phases, denoted as polymorphs.[3,6] Among these polymorphs, stable, metastable, or unstable phases may exist, and a stable phase must have the lowest surface free energy thermodynamically.[7,8] When thermodynamic conditions change, the crystal structure will transform with free energy variation but chemical composition scarcely changed, called phase transition.[9,10] For phase transition, nanocrystal structure has a characteristic change direction, and change of physical properties is demonstrated, such as electrical conductivity and optical adsorption, which allows for modulating function-oriented

Received: December 18, 2018
Published: February 12, 2019

DOI: 10.1021/acs.accounts.8b00645
Acc. Chem. Res. 2019, 52, 780−790

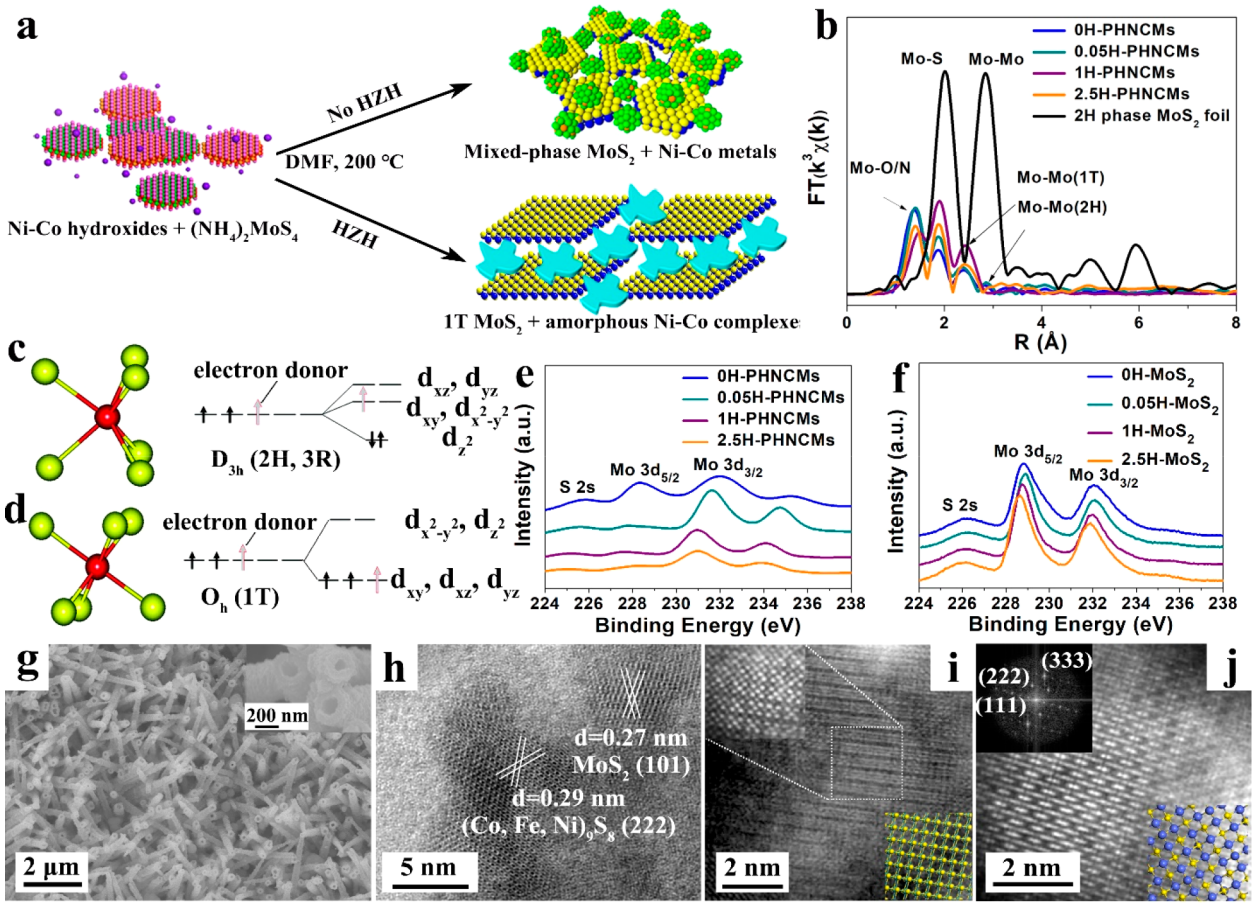

Figure 1. (a) Schematic illustration showing phase transition of MoS_2 through HZH induction and Ni−Co compound assistance. (b) EXAFS data for PHNCMs with different amounts of HZH. Reproduced with permission from ref 23. Copyright 2017 Nature Publishing Group. Simplified representations for crystal field theory of Mo 4d states of (c) 2H MoS_2 and (d) 1T MoS_2. Reproduced with permission from ref 25. Copyright 2011 American Chemical Society. (e, f) XPS spectra for PHNCMs and MoS_2 nanosheets, respectively, with different amounts of HZH. Reproduced with permission from ref 23. Copyright 2017 Nature Publishing Group. (g) Scanning electron microscopy (SEM), (h) high-resolution TEM (HRTEM), and (i, j) AC-STEM images and corresponding structural model of 1T′ MoS_2 and $(Co,Fe,Ni)_9S_8$ in FeCoNi-HNTAs, respectively. Reproduced with permission from ref 26. Copyright 2018 Nature Publishing Group.

behaviors for practical applications.[9,11] Therefore, nanocrystals in a specific phase can be constructed for particular investigative purposes, defined as phase engineering.

Substantial demands have been affiliated with property explorations and practical utilizations for desirable nanocrystals through phase engineering, which provides the guideline for phase-controlled synthesis.[9,11] Phase-based novel nanostructures, like heterophase materials, have emerged for modulation of catalysis and feasibility in fine chemical industries.[12−14] Abundant synthetic strategies have been studied for phase engineering, divided into top-down and bottom-up methods.[6,9−11,15] The top-down method is mainly exfoliation from bulk counterparts for synthesis of transition metal dichalcogenides (TMDCs), producing high-quality metallic TMDCs nanosheets, but this method is low-yield, producing unstable products with uncontrollable size and morphology, and hinders development.[6,9] Bottom-up methods include solvothermal, vapor-phase, and temperature-based synthesis, etc. Solvothermal strategies enable large-scale controllable synthesis of well-defined nanocrystals with phase engineering, but impurities and product repeatability need to be tackled.[2,8,9,11,16] Vapor-phase methods contribute to high-quality nanocrystals with clean surfaces and uniform size and morphology, but high cost and small-scale production impede scale-up utilization.[9,17,18] Temperature-based synthesis is scarcely used to generate well-defined nanocrystals with phase modulation at an ultrathin scale, which results in large-sized products and high energy consumption.[2,19] On the other side, phase stability is a vital issue for mass production and utilization, providing an opportunity to meet practical requirements. It is common that a metastable phase possesses more satisfactory behavior in some applications, but the metastable nature restricts sustained functionality and long-term characteristics.[7−10] Therefore, excellent phase stability facilitates in-depth exploration and overall understanding of polymorphs.

In this Account, we will overview our recent progress in developing inorganic nanocrystals with phase engineering and discuss critical effects on phase stability. From the perspective of regulating nucleation and growth at an ultrathin scale, we summarize several phase-controlled synthetic strategies in solvothermal systems, through which we control limited chemical bonds and overcome low energy barriers to achieve phase engineering. Afterward, in-depth insights into phase stability are demonstrated by critical factors. The modulation at an ultrathin scale has been emphasized for phase control in inorganic nanocrystals. We then highlight coverage-dependent electronic structures and cooperative chemisorption of TiO_2(B) nanomaterials by ligand-induced surface interactions.

DOI: 10.1021/acs.accounts.8b00645
Acc. Chem. Res. 2019, 52, 780−790

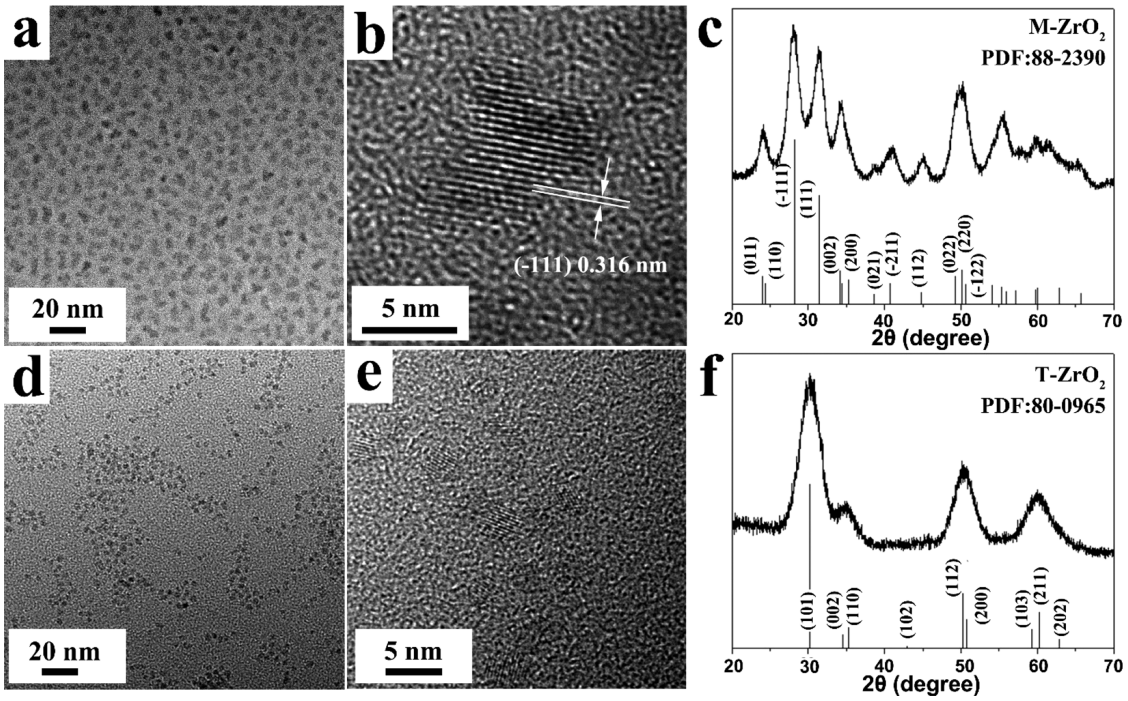

Figure 2. TEM and HRTEM images and X-ray diffraction (XRD) patterns of (a, b, c) M-ZrO_2 nanocrystals and (d, e, f) T-ZrO_2 nanocrystals. Reproduced with permission from ref 33. Copyright 2009 Springer Link.

In addition, an overall water splitting (OWS) system reveals the impacts of phase-engineered MoS_2-based nanomaterials on electrocatalytic performance. Finally, we put forward the outlook for future development prospects.

2. PHASE-CONTROLLED SYNTHESIS OF INORGANIC NANOCRYSTALS

Accessible and controllable methodologies for preparation of inorganic nanocrystals with phase engineering are regarded as the cornerstone for novel discoveries of properties and practical applications. In this section, we summarize several phase-controlled syntheses for MoS_2, ZrO_2, In_2O_3, and TiO_2 nanocrystals, including electron-donor induction, solvent modulation, dissolution−recrystallization, and secondary ion incorporation methods, with the view of modulating the nucleation and growth of nanocrystals at an ultrathin scale.

2.1. Electron-Donor Induction Method

TMDCs are considered as significant graphene-like two-dimensional nanomaterials due to their excellent behavior in catalysis, energy storage, sensing, and electronic devices.[6,20,21] Here we regard MoS_2 as the main object for discussion. The crystal structures of MoS_2 are divided into trigonal prismatic and octahedral symmetries, corresponding to semiconducting 2H or 3R phases and metallic 1T phase, respectively.[9,10] Compared to its 2H counterpart, 1T MoS_2 allows for superior electron transport kinetics and increased density of active sites for HER.[15,20] For electronic structures, 2H MoS_2 exhibits completely filled 4d orbitals; nevertheless partially filled 4d orbitals result in metallic features of 1T MoS_2.[22] The electronic structures can be tuned by electron donors to achieve phase transition. At present, the commonly applied technique for synthesizing 1T MoS_2 is lithium-assisted exfoliation from the bulk 2H counterpart.[15,20] However, it is difficult to obtain high-yield stable 1T MoS_2 with uniform size and morphology. Recently, potassium-assisted chemical vapor deposition methods have been developed for the synthesis of high phase-purity crystals and monolayers of metallic Mo chalcogenides.[17,18] But there are scarcely electrochemical stability consequences of 1T′ MoS_2.

We have achieved complete phase transition of MoS_2 using Ni−Co hydroxides as precursors with hydrazine hydrate (HZH) induction, obtaining porous hybrid nanostructures comprised of amorphous Ni−Co complexes and 1T MoS_2, denoted as PHNCMs (Figure 1a).[23] We utilized HZH as an electron donor to transfer the electron into Mo 4d orbitals and induce phase transition from 2H to 1T phase.[22] The extended X-ray absorption fine structure (EXAFS) spectrum shows the phase transition process (Figure 1b) with increasing amount of HZH (samples denoted as xH-PHNCMs and xH-MoS_2, x stands for the added HZH volume in milliliters). When the quantity of HZH reaches 1 mL, mix-phased 2H and 1T MoS_2 completely transforms to pure 1T phase with distinct Mo−Mo bond length and XPS peak positions.[6,24] In the view of crystal field theory, the Mo 4d orbitals of 2H MoS_2 with a D_{3h}-MoS_6 unit are divided into three symmetry-induced groups: (1) Mo $4d_{z^2}$, completely occupied state; (2) Mo $4d_{xy}$ and Mo $4d_{x^2-y^2}$; and (3) Mo $4d_{xz}$ and Mo $4d_{yz}$, unoccupied state (Figure 1c). For 1T MoS_2, the Mo 4d orbitals of an O_h-MoS_6 are divided into two groups: (1) Mo $4d_{xy}$, $4d_{yz}$, and $4d_{xz}$, occupied by two electrons, and (2) Mo $4d_{z^2}$ and Mo $4d_{x^2-y^2}$, unoccupied state (Figure 1d). The partial occupation of Mo $4d_{xy}$, $4d_{yz}$, and $4d_{xz}$ orbitals in 1T MoS_2 results in the metallic property, but it also makes 1T MoS_2 unstable. Therefore, if there is an additional electron occupying the Mo $4d_{xy}$, $4d_{yz}$, and $4d_{xz}$ orbitals, it will increase the stability of 1T MoS_2 because of half-filled 4d orbitals occupied by single-spin electrons. In contrast, when such phenomenon occurs in 2H MoS_2, the electrons that occupy the Mo $4d_{xy}$, $4d_{yz}$, and $4d_{xz}$ orbitals and Mo $4d_{x^2-y^2}$ orbitals lead to metallic nature, but it makes 2H MoS_2 destabilize due to the single occupied states of the 4d orbitals.[25] Therefore, if there is an electron donor in the

DOI: 10.1021/acs.accounts.8b00645
Acc. Chem. Res. 2019, 52, 780−790

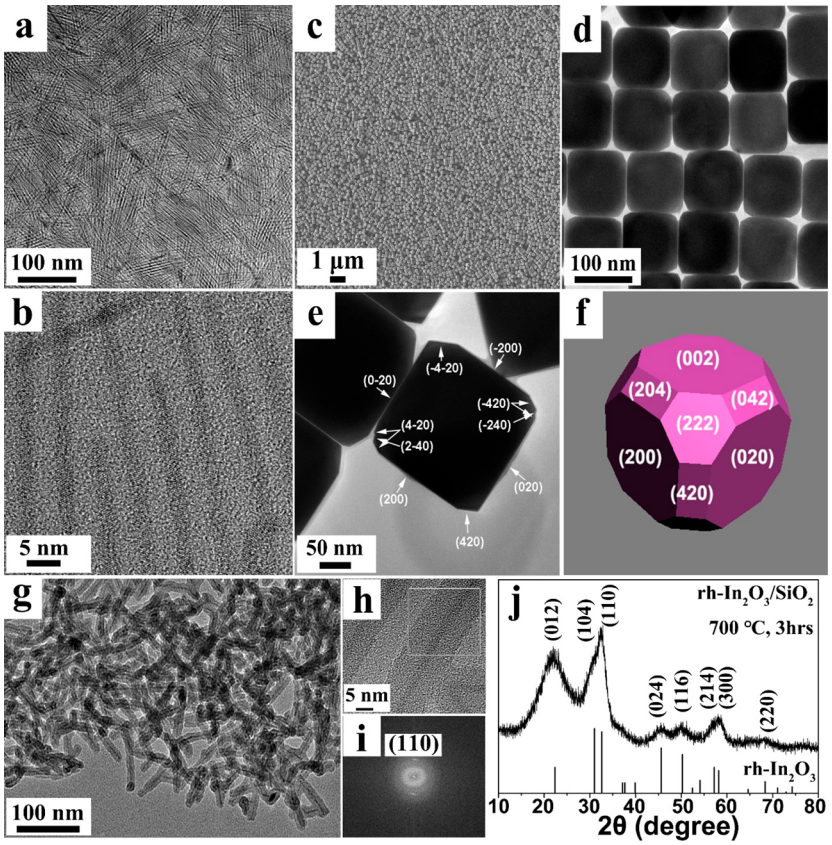

Figure 3. (a) TEM and (b) HRTEM images of InOOH UNWs. (c) SEM, (d) TEM, and (e) HRTEM images and (f) crystal model of truncated c-In_2O_3 nanocubes. (g) TEM, (h) HRTEM, (i) fast Fourier transform (FFT) images, and (j) XRD pattern of rh-In_2O_3/SiO_2 nanowires. Reproduced with permission from ref 38. Copyright 2009 American Chemical Society.

reaction system, the production and stability of 1T MoS_2 can be achieved. The comparison between X-ray photoelectron spectroscopy (XPS) spectra of PHNCMs and MoS_2 nanosheets with different amounts of HZH (Figure 1e,f) confirms that the phase transition to pure 1T phase must occur with amorphous Ni−Co complexes. Expanding this reaction system, we constructed a hybrid nanotube-array electrode constituted by 1T′ MoS_2 and $(Co,Fe,Ni)_9S_8$ (FeCoNi-HNTAs) with Fe,Co,Ni-based layered double hydroxide (LDH) nanowire arrays as templates (Figure 1g,h).[26] The compositions are confirmed by atomic resolution aberration-corrected scanning transmission electron microscopy (AC-STEM) images (Figure 1i,j). For this approach, HZH alone could not contribute to pure 1T MoS_2, and hydroxides or LDH played an essential role in phase transition. On the basis of the metastable nature of 1T MoS_2 that is easily transformed to 2H phase,[18] we think the secondary components in our hybrid nanomaterial systems could stabilize 1T MoS_2, which is clarified in detail in section 3.1. The hydroxides or LDH coordinate with HZH to generate amorphous complexes, which may have interactions with as-formed 1T MoS_2 through probable electrostatic forces[24,27] or strain effects.[7] A facile strategy has been developed for phase engineering of MoS_2 through modulating growth and electronic structures at an ultrathin level.

2.2. Solvent Modulation Method

ZrO_2 nanocrystal has been widely investigated as a commendable catalyst and catalytic support.[28,29] ZrO_2 polymorphs demonstrate monoclinic, tetragonal, and cubic phases (M-ZrO_2, T-ZrO_2, and C-ZrO_2), and different phases vary in their catalytic behaviors.[30] Ji and co-workers synthesized mixed M-ZrO_2 and T-ZrO_2 nanocrystals with well-controlled size and morphology.[5] The ratio of M-ZrO_2 in products reduces when hydrocarbon chain length of organic acids as solvents is increased. However, pure T-ZrO_2 nanocrystals have not been obtained owing to their metastable nature and martensitic phase transformation from T-ZrO_2 to M-ZrO_2.[31,32] We have developed monodisperse pure M-ZrO_2 (Figure 2a,b) and T-ZrO_2 (Figure 2d,e) nanocrystals by solvent modulation.[33] Short-chain alcohols, like ethanol and butanol, result in M-ZrO_2 (Figure 2c), while long-chain alcohols, such as hexanol, lead to T-ZrO_2 (Figure 2f). Alternative mechanisms, pyrolysis and esterification−hydrolysis, enable phase-selected growth of T-ZrO_2 and M-ZrO_2 nucleation respectively, which is different from size-dependent T-ZrO_2-to-M-ZrO_2 martensitic transformation where the ratio of M-ZrO_2 increases with increasing size.[5,16] Amorphous precursor was separated before ZrO_2 nucleation because the occurrences of T-ZrO_2 nucleation and martensitic transformation are immediate and simultaneous. In addition, T-ZrO_2 ultrathin nanowires (UNWs) were prepared, originating from oriented attachment with facet-selected adsorption of oleylamine. In this work, we achieve phase-controlled synthesis of ZrO_2 nanocrystals by controlling nucleation and growth based on precursors in a specific phase with solvent modulation, providing the basis of catalyst design.

2.3. Dissolution−Recrystallization Method

It is intriguing to spotlight phase engineering with dimensional variation. In_2O_3 nanocrystals are polymorphous semiconduc-

DOI: 10.1021/acs.accounts.8b00645
Acc. Chem. Res. 2019, 52, 780−790

tors, exhibiting cubic phase (c-In_2O_3), corundum-type (rh-In_2O_3) phase, and Rh_2O_3-II-type phase, which are applied in solar cells,[34] gas sensors,[35] and catalysis.[36] Annealing−dehydration strategy was widely used for the synthesis of rh-In_2O_3 and c-In_2O_3 from InOOH and $In(OH)_3$, respectively.[37] However, this research seldom achieved well-controlled size, morphology, and surface features. Meanwhile, the phase transition mechanism of InOOH to c-In_2O_3 to rh-In_2O_3 remains ambiguous. Our group developed a facile synthesis of c-In_2O_3 and rh-In_2O_3 nanocrystals from InOOH UNWs (Figure 3a,b).[38] A dissolution−recrystallization process is demonstrated to form c-In_2O_3 nanocubes instead of rh-In_2O_3 nanocrystals. The InOOH UNWs decompose and dissolve into the solvent at the start, and c-In_2O_3 crystal nuclei originate and aggregate, forming single-crystal c-In_2O_3 precubes and the final truncated nanocubes by Ostwald ripening (Figure 3c−f). To impede the dissolution process, the morphology freezing method is deployed to prepare rh-In_2O_3 nanowires. SiO_2 coats the surface of InOOH UNWs for the annealing process and rh-In_2O_3/SiO_2 nanowires can be obtained (Figure 3g−j). We speculate for this transition that one possible mechanism is that the dehydration of InOOH leads to high water pressure in the core−shell structure and the other is that the interface strain of core−shell reconstruction gives rise to the transition. It is pivotal to control the growth of ultrathin nuclei. Both of the two methods need to start from corresponding ultrathin precursors, achieving the transformation with lower energy barrier. These strategies facilitate the understanding and control of phase transition and stability regarding the restraint of size and surface in the low dimensional nanoscale.

2.4. Secondary Ion Incorporation Method

TiO_2 is a significant semiconductor with unique optical adsorption properties for energy conversion and environmental protection.[2] Titania-based nanomaterials have been developed for photovoltaics and photocatalysis, especially for dye-sensitized solar cells and photocatalytic HER.[39] Three polymorphs emerge: anatase, brookite, and rutile. Wu et al. synthesized TiO_2 nanocrystals in pure anatase and rutile phases through adjusting inorganic acidic solvents.[40] But high temperature and long reaction time made as-prepared nanocrystals aggregate in large size. A modified sol−gel method was developed for preparation of anatase nanocrystals at a low temperature.[41] Nevertheless, excessively long reaction time and irregular morphology of products are unfavorable. Moreover, phase transition from anatase to rutile only occurred above 600 °C; thus pure rutile phase could not be achieved with ease.[11]

Phase-controlled syntheses of pure rutile and anatase nanocrystals were performed by introducing Sn^{4+} ions.[42] With increasing amount of Sn^{4+} ions, TiO_2 nanocrystals experienced phase transition from pure anatase to pure rutile, which demonstrated remarkable regulatory effects of Sn^{4+} ions that scarcely change the crystal structure of products (Figure 4a,b). Mild condensation of hydrolysis products and subsequent phase separation of nanocrystals from bulk solvent by gravity contribute to monodisperse TiO_2 nanoparticles with uniform and narrow size distribution. As different from phase transition based on bulk material with high reaction temperatures, we utilized Sn^{4+} ions and $TiCl_3$ in ethanol to control the mild nucleation. Combined with the synthesis of Mo_5N_6 nanosheets by Ni ion induction from Qiao's group,[43] secondary ion induction provides the possibility for modulation of phase ratios and compositions of products, which facilitates application-oriented and controllable syntheses of nanocrystals in desirable phases.

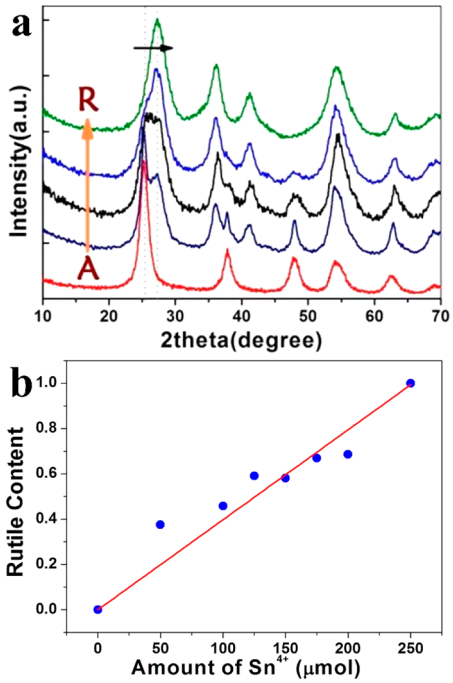

Figure 4. (a) XRD patterns from anatase to rutile by increasing the amount of Sn^{4+} and (b) corresponding relationship of the rutile content and amount of Sn^{4+}. Reproduced with permission from ref 42. Copyright 2012 WILEY-VCH.

3. PHASE STABILIZATION EFFECTS

In-depth understanding of phase stability of inorganic nanocrystals is meaningful to reveal the mastery of growth and phase transition, which is fundamental to their widespread utilization. Since the 1970s, thermodynamic phase stability of polymorphs has emerged for explorations.[31,44] At present, the studies on phase stability of transition metals and their oxides and chalcogenides are extensive for novel properties and practical value.[5,9−11,13,14,37] However, a detailed discussion has not been realized in this field. In this section, we will mainly discuss critical factors influencing phase stability, which are secondary component incorporation, strain−size, cationic doping, and agent capping effects.

3.1. Secondary Component Incorporation

It is well-known that 2H MoS_2 (representing group-VIB TMDCs) is thermodynamically stable, while the 1T counterpart is metastable and preferentially converted to 2H phase.[9,10] Strain effects,[7] electron donating effects,[22] and electrostatic forces[24,27] positively stabilize 1T MoS_2. But phase stability during catalysis has been neglected all the time. In our recent work, excellent phase stability of 1T MoS_2 during water splitting has been achieved by secondary component incorporation.[23,26] We deployed oxygen evolution reaction (OER) measurements for comparison of XPS spectra before and after OER because of the easy *in situ* oxidation of electrocatalysts during OER. The XPS spectra (Figure 5a,b) indicate the invariability of 1T MoS_2 in PHNCMs and *in situ* oxidation of MoS_2 nanosheets after OER, which precisely confirms the stabilization effects of the secondary component. Advanced technology has been used to prove phase stability of

DOI: 10.1021/acs.accounts.8b00645
Acc. Chem. Res. 2019, 52, 780−790

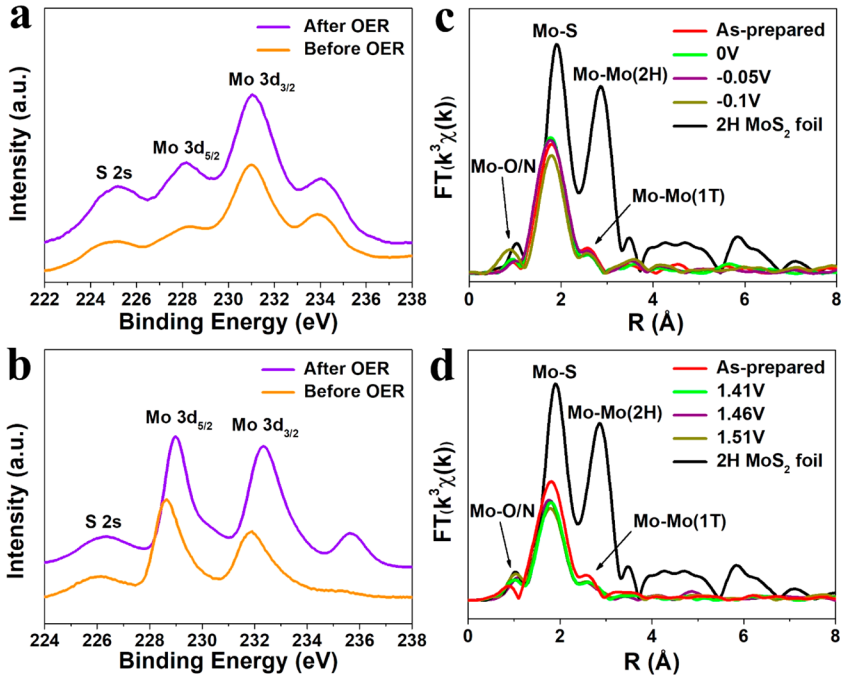

Figure 5. XPS spectra of (a) PHNCMs and (b) MoS_2 nanosheets before and after OER. Reproduced with permission from ref 23. Copyright 2017 Nature Publishing Group. (c, d) *In situ* EXAFS data recorded on FeCoNi-HNTAs for HER and OER, respectively. Reproduced with permission from ref 26. Copyright 2018 Nature Publishing Group.

1T MoS_2 during electrocatalysis. We carried out *in situ* EXAFS for FeCoNi-HNTAs at different potentials during HER and OER (Figure 5c,d). The peak positions of Mo−Mo bond for 1T MoS_2 were immobile in contrast to the initial ones, which illustrated remarkable phase stability. Compared to unstable 1T MoS_2 from exfoliation, we used the interaction in molecular level between the two components to acquire stable 1T MoS_2 for practical applications.

3.2. Strain−Size Effect

A critical size effect has a vital influence on phase stability of ZrO_2 nanocrystals, above which (~30 nm) metastable T-ZrO_2 transforms to M-ZrO_2 at various temperatures, and T-ZrO_2 is stable below 10 nm at room temperature.[31,45] Size distribution of T-ZrO_2 and M-ZrO_2 below 10 nm provides fascinating understanding of phase stability from our work. We have used Williamson−Hall equation[46] to investigate the relationship between effective strain and crystal size.[33] Figure 6 shows that the compressive strain increases when the nanocrystal size decreases for M-ZrO_2. In contrast, the effective strain of T-ZrO_2 remains near zero, indicating that T-ZrO_2 is unconstrained. Compared to T-ZrO_2, M-ZrO_2 possessed larger compressive strain in the size range below 8 nm. Therefore, we deliver the straightforward proof that strain effect makes T-ZrO_2 more stable than M-ZrO_2 in restrictive sizes. The compressive strain displays a rapid enlargement when the size of M-ZrO_2 is below 5 nm, which accounts for the unattainable realization of M-ZrO_2 with size below 2.8 nm experimentally. Besides, there is no martensitic transformation regarding stable T-ZrO_2 nanocrystals in this size range.[32] At an ultrathin scale, ZrO_2 nanocrystals exhibit novel stability rules, and the relationship between size and strain enables the possibility to synthesize pure-phased T-ZrO_2 and M-ZrO_2 ultrathin nanocrystals.

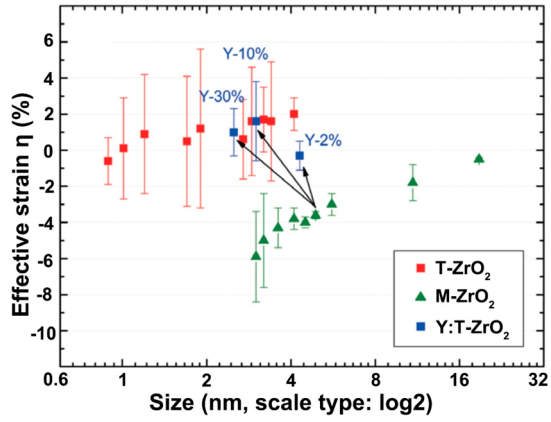

Figure 6. Relationship between effective strain and size for T-ZrO_2, M-ZrO_2, and Y-doped T-ZrO_2. The arrows indicate M-ZrO_2 precursor for the synthesis of Y-doped T-ZrO_2. Reproduced with permission from ref 33. Copyright 2009 Springer Link.

3.3. Cationic Doping

Cationic doping facilitates achievement of inorganic nanocrystal diversification. Generally, cations with smaller size and lower oxidation state than Ti^{4+} accelerate phase transition from anatase to rutile of TiO_2 due to the enhancement of oxygen vacancies with substitution of Ti^{4+} ions by lower-valence cations. As a result, the rigid oxygen sublattice becomes modifiable rather than inert, which affects the crystal structure and facilitates the modulation of chemical bonds to produce rutile phase. Conversely, cation substitution with higher oxidation state than Ti^{4+} leads to the disappearance of available oxygen vacancies, which degenerates the regulation of the structure.[11,47] Banfield and co-workers demonstrated that yttrium (Y) generated Y−O clusters on the surfaces of anatase and modulated the interfacial and surface free energy, obstructing the growth of anatase and thus stabilizing this

DOI: 10.1021/acs.accounts.8b00645
Acc. Chem. Res. 2019, 52, 780−790

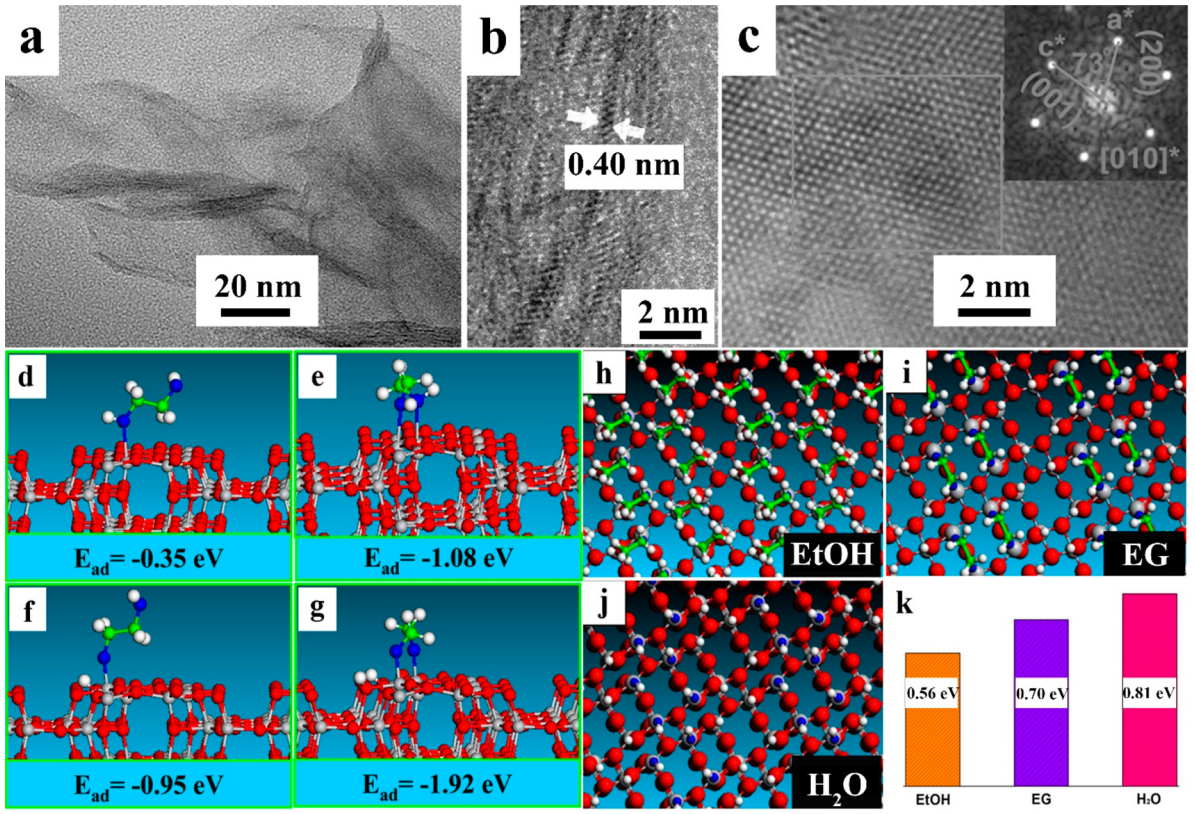

Figure 7. (a) TEM, (b) HRTEM, and (c) AC-STEM images of TiO_2(B) nanosheets. Adsorption models and free energies of EG on TiO_2(B) (010) lattice faces from DFT calculations: (d) monodentate, (e) bidentate, (f) dissociative monodentate, and (g) dissociative bidentate adsorption. Saturated adsorption of different agents on TiO_2(B) (010) planes from DFT calculations: (h) ethanol, (i) EG, (j) water. (k) Free energies of adsorption. Reproduced with permission from refs 51 and 55. Copyright 2013 Nature Publishing Group and 2018 American Chemical Society.

phase up to 700 °C.[48] We introduce yttrium oleate into the M-ZrO_2 synthesis at the initial stage to modulate the nucleation and growth at an ultrathin scale and obtained Y-doped T-ZrO_2 nanocrystals. If yttrium oleate is added in the ripening stage of M-ZrO_2 nanocrystals, the monoclinic phase was retained. In this approach, Y-doping behavior hardly changes the crystal structure of T-ZrO_2 nanocrystals.[33] The effective strain of 2% Y-doped T-ZrO_2 locates between T-ZrO_2 and M-ZrO_2 gap, whereas 10% and 30% Y-doped T-ZrO_2 maintained similar strain level with T-ZrO_2 (Figure 6). This result reveals that Y-doping can mitigate the compressive strain of ZrO_2 nanocrystals gradually, inducing the transformation from M-ZrO_2 to T-ZrO_2. We believe cationic doping benefits regulation of phase stability at the atomic scale.

3.4. Agent Capping Effect

Phase stability usually depends on thermodynamics, especially when the size is below 10 nm or even below 1 nm.[8] At this scale, surface energy determines phase stability. Three polymorphs of TiO_2 show varied stability in different size ranges. Rutile is the most stable when size is above 35 nm, while anatase exhibits superior stability when size is below 11 nm.[11] Besides surface energy, several additives also have positive effects on phase stability, such as surfactants, ions, and polymers.[49] Phase stability can be modified by altering surface states and achieved by surface interaction between surface and additives.

We synthesized TiO_2(B) ultrathin nanosheets, a metastable phase of TiO_2, in an ethylene glycol (EG) solvent system.[50] Surface adsorption of different solvents on TiO_2(B) was studied to demonstrate phase stability mechanism.[51] The ultrathin TiO_2(B) nanosheets (Figure 7a,b) preferentially expose (010) lattice facets (Figure 7c). Density functional theory (DFT) calculations (Figure 7d–g) show that bidendate adsorption in the dissociative models is the most favorable and stable type. In saturated Ti adsorption models, water possesses larger free energy, so it can replace EG to adsorb on TiO_2(B) (010) planes (Figure 7h–k); consequently a small amount of water leads to phase transition from TiO_2(B) to anatase. Monodentate ethanol causes larger steric interaction, resulting in lower free energy. We provide a concept that surface-specific interaction by structure-match configuration stabilizes TiO_2(B) with the high-energy facet exposed at the molecular level.

4. PHASE ENGINEERING EFFECTS ON PROPERTIES AND APPLICATIONS

4.1. Ligand-Induced Molecule–Surface Interactions

For investigating novel properties of ultrathin nanocrystals with phase engineering, we demonstrate ligand-induced molecule–surface interactions for TiO_2(B) nanosheets. When size is reduced to atomic scale, it is easier to modify the surface of TiO_2 ultrathin nanosheets with ligands.[52] With large surface-to-volume ratio and high surface energy, a dominant contribution of the nanomaterial surface is demonstrated in physical and chemical processes. Atomically thin two-dimensional nanomaterials have emerged as ideal model platforms for studying nanoscale surface chemistry and applications because of the high ratios of surface atoms and restrictive dimensions.[53,54] Using one-unit-thin TiO_2 nano-

DOI: 10.1021/acs.accounts.8b00645
Acc. Chem. Res. 2019, 52, 780–790

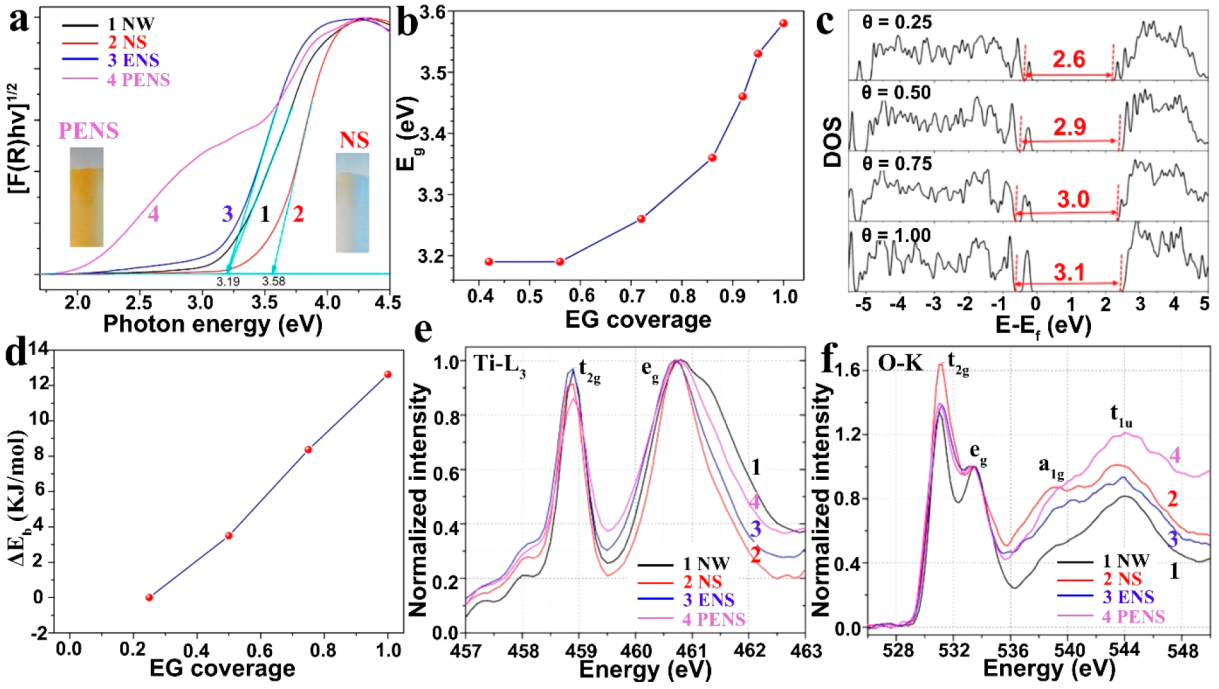

Figure 8. (a) Absorption spectra of 1-NWs, 2-NSs (EG coverage θ_{EG} = 1.00), 3-ENSs (θ_{EG} = 0.42), and 4-PENSs. (b) Relationship of band gaps to EG coverages of TiO_2(B) NSs. (c) Total DOS of TiO_2(B) NSs dependent on EG coverages and the band gaps based on DFT calculations. (d) The relationship between Ti−O bonding energies (E_b) and EG coverages. The zero point is set at θ = 0.25. (e, f) EXAFS spectra of Ti L_3 and O K edges. Reproduced with permission from ref 55. Copyright 2018 American Chemical Society.

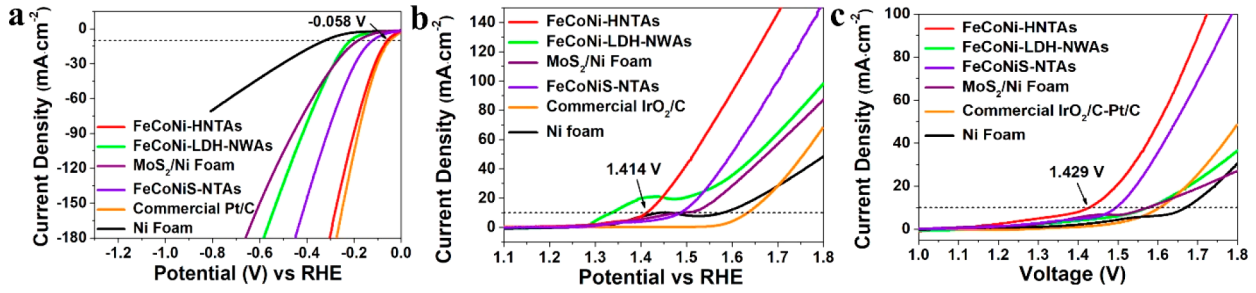

Figure 9. Polarization curves for (a) HER, (b) OER, and (c) OWS recorded on FeCoNi-HNTAs, respectively. Reproduced with permission from ref 26. Copyright 2018 Nature Publishing Group.

sheets as a model platform in this section, we will reveal the electronic mechanisms of how surface ligands interact with nanomaterials and modify their electronic structures and properties. Our group deployed TiO_2(B) nanowires (NWs), EG-modified nanosheets (NSs), etched nanosheets (ENSs), and peroxide-modified etched nanosheets (PENSs) to show the relationship between electronic structure and EG coverages.[55] Different electronic band gaps of NSs and ENSs indicate EG coverage can affect band gap (Figure 8a). Figure 8b shows the detailed correlation between band gaps and EG coverages, which proves the band gaps increase with increased EG coverage, and surface ligation states can govern electronic structures at a high coverage. TiO_2(B) nanosheets with varied EG coverage were also the models to evaluate coverage-dependent band gaps based on density of states (DOS). The calculated band gaps were also enhanced with increased EG coverage (Figure 8c). In addition, the bonding energies of Ti−O reveal a positive increase with increased EG coverage (Figure 8d). From EXAFS spectra, the peak width of the e_g band and the intensity ratio of t_{2g} to e_g ($I_{t_{2g}}/I_{e_g}$) correspond to the localized and delocalized bonding features of Ti 3d atomic orbitals (AOs) and the ratios of Ti 3d and O 2p orbitals in the unoccupied electronic states, respectively (Figure 8e,f). Compared with NWs as the bulk counterpart, the peak width of e_g and peak intensity of t_{2g} become narrowed and degenerated, indicating the redistributions of Ti 3d AOs from energy bands to surface coordination bonds. On one hand, the ultrathin scale avoids long-range lattice periodicity to impede the delocalization of $4d_{z^2}$ orbitals that can form e_g bands. On the other hand, ENSs possess broader e_g peak than NSs, suggesting that surface ligands can hinder the delocalization of $4d_{z^2}$ orbitals and thus constrict e_g bands. The decrease of Ti L_3 ratio of $I_{t_{2g}}/I_{e_g}$ and increase of O K ratio of $I_{t_{2g}}/I_{e_g}$ for NSs compared with NWs reveal the reduced density of unoccupied Ti 3d π states and increased ratios of unoccupied O 2p π states. Therefore, the coordination of EG ligands is through overlapping O 2p π with Ti 3d π orbitals, contributing to the polarization of Ti 3d π AOs and suppressing delocalization into the lattices for formation of t_{2g} bands. These novel phenomena provide the electronic explanation for size-reduced and ligand-induced effects on surface interactions.

DOI: 10.1021/acs.accounts.8b00645
Acc. Chem. Res. 2019, 52, 780−790

4.2. Water Splitting Electrocatalysis

Here we mainly illustrate phase-engineered MoS_2-based nanocrystals for water splitting, discussing phase engineering effects on electrocatalysis. PHNCMs with pure 1T MoS_2 achieve lower overpotentials, superior kinetics, excellent conductivity, and long-term durability for water splitting electrocatalysis compared to PHNCMs with mixed 2H and 1T MoS_2.[23] It is noteworthy that FeCoNi-HNTAs (including pure 1T′ MoS_2) demonstrated ultrahigh activity for OWS.[26] The overpotentials at 10 mA cm^{-2} are just 58 and 184 mV (Figure 9a,b) for HER and OER, respectively. In a two-electrode configuration, we utilized FeCoNi-HNTAs as anode and cathode simultaneously for OWS, achieving extremely low voltage of 1.429 V at 10 mA cm^{-2} (Figure 9c). Systematic design of this electrode enhances electrocatalytic performance: plentiful active sites for HER and excellent conductivity of 1T′ MoS_2, synergistic effects among Fe, Co, and Ni ions for enhancing intrinsic OER activity, and the superaerophobicity and superhydrophilicity of electrode surface for fast mass transfer. Several comparisons of bifunctional electrocatalysts with leading performances for OWS are made for demonstrating superior electrocatalytic ability of FeCoNi-HNTAs[15,20,56,57] (cell voltage to hold 10 mA cm^{-2} for OWS based on Ni foam in 1.0 M KOH electrolyte: Pt/C-IrO_2, 1.71 V; $Fe_{10}Co_{40}Ni_{40}P$, 1.57 V; MoS_2/Ni_3S_2, 1.56 V; $Ni_xCo_{3-x}S_4/Ni_3S_2$, 1.53 V; h-NiS_x, 1.47 V; MoO_x/Ni_3S_2, 1.45 V; etc.). It is believed that phase engineering holds a great promise of an essential boost for OWS and creates a new road to construct high-efficiency electrocatalysts.

5. SUMMARY AND OUTLOOK

This Account summarizes numerous recent achievements in phase-engineered synthetic methodologies and stabilization effects on inorganic ultrathin nanocrystals. Accessible and manageable synthetic strategies show fine-tuned nucleation and growth of high-quality nanocrystals at an ultrathin scale. In the synthetic process, the introduction of specific ions, solvents, and other functional components has a pivotal influence on the lattice strain or surface free energy, thus affecting phase stability. Discussions have been focused on structures, sizes, morphologies, compositions, and surface modifications of ultrathin nanocrystals, which play significant roles in further function explorations. New discoveries of electronic properties and remarkable catalytic performance provide in-depth insights into exploration and feasibility of inorganic nanomaterials with phase engineering for practical applications.

Although great progress has been made in this field, explorations on phase design and construction still need to continuously step forward. Preferable synthetic strategies that make for producing nanocrystals in expected phase with a sophisticated level of size, morphology, and component adjustment are eagerly awaited. Meanwhile, large-scale production for industrial and social deployment is also significant. It is necessary to design appropriate reaction routes, modulate the reaction parameters, and assess the feasibility of obtained materials. With the rapid development of material characterization technologies, it is promising to *in situ* characterize the process of phase transition to gain comprehensive mechanistic understanding. The unambiguous mastery of phase transition mechanism is conducive to precisely control the process and degree of phase transition, acquiring expected materials. In conclusion, we hope phase engineering and stability of inorganic ultrathin nanocrystals will be well developed in the future so that more satisfactory materials and novel phenomena can be substantially uncovered.

AUTHOR INFORMATION

Corresponding Author

*E-mail: wangxun@mail.tsinghua.edu.cn.

ORCID

Xun Wang: 0000-0002-8066-4450

Funding

This work was financially supported by China Ministry of Science and Technology under Contracts 2017YFA0700101 and 2016YFA0202801 and National Natural Science Foundation of China (Grants 21431003 and 21521091).

Notes

The authors declare no competing financial interest.

Biographies

Haoyi Li obtained his Bachelor of Science from College of Science, Beijing University of Chemical Technology, in 2014 majoring in Applied Chemistry. He is currently pursuing a Ph.D. degree in Department of Chemistry, Tsinghua University, under supervision of Prof. Xun Wang. His research interests focus on controllable synthesis of hybrid nanomaterials based on transition metal dichalcogenides with phase engineering and their electrocatalytic applications.

Xun Wang studied in Northwest University of China as undergraduate and postgraduate student during 1994−2001 and received his Ph.D. from Department of Chemistry, Tsinghua University, in 2004. He then joined the faculty of Department of Chemistry, Tsinghua University, and was promoted to associate professor and full professor in 2005 and 2007, respectively. His current research interests concentrate on synthesis, self-assembly, and applications of sub-nanometer ultrathin nanocrystals.

REFERENCES

(1) Atou, T.; Kusaba, K.; Fukuoka, K.; Kikuchi, M.; Syono, Y. Shock-induced phase transition of M_2O_3 (M = Sc, Y, Sm, Gd, and In)-type compounds. *J. Solid State Chem.* **1990**, *89*, 378−384.

(2) Chen, X.; Mao, S. S. Titanium dioxide nanomaterials: synthesis, properties, modifications, and applications. *Chem. Rev.* **2007**, *107*, 2891−2959.

(3) Chen, Y.; Fan, Z.; Zhang, Z.; Niu, W.; Li, C.; Yang, N.; Chen, B.; Zhang, H. Two-Dimensional Metal Nanomaterials: Synthesis, Properties, and Applications. *Chem. Rev.* **2018**, *118*, 6409−6455.

(4) Heising, J.; Kanatzidis, M. G. Structure of restacked MoS_2 and WS_2 elucidated by electron crystallography. *J. Am. Chem. Soc.* **1999**, *121*, 638−643.

(5) Zhao, N.; Pan, D.; Nie, W.; Ji, X. Two-Phase Synthesis of Shape-Controlled Colloidal Zirconia Nanocrystals and Their Characterization. *J. Am. Chem. Soc.* **2006**, *128*, 10118−10124.

(6) Chhowalla, M.; Shin, H. S.; Eda, G.; Li, L.-J.; Loh, K. P.; Zhang, H. The chemistry of two-dimensional layered transition metal dichalcogenide nanosheets. *Nat. Chem.* **2013**, *5*, 263−275.

(7) Duerloo, K. A.; Li, Y.; Reed, E. J. Structural phase transitions in two-dimensional Mo- and W-dichalcogenide monolayers. *Nat. Commun.* **2014**, *5*, 4214.

(8) Finnegan, M. P.; Zhang, H.; Banfield, J. F. Phase stability and transformation in titania nanoparticles in aqueous solutions dominated by surface energy. *J. Phys. Chem. C* **2007**, *111*, 1962−1968.

DOI: 10.1021/acs.accounts.8b00645
Acc. Chem. Res. 2019, 52, 780−790

(9) Li, H.; Jia, X.; Zhang, Q.; Wang, X. Metallic Transition-Metal Dichalcogenide Nanocatalysts for Energy Conversion. *Chem.* **2018**, *4*, 1510−1537.
(10) Voiry, D.; Mohite, A.; Chhowalla, M. Phase engineering of transition metal dichalcogenides. *Chem. Soc. Rev.* **2015**, *44*, 2702−2712.
(11) Hanaor, D. A. H.; Sorrell, C. C. Review of the anatase to rutile phase transformation. *J. Mater. Sci.* **2011**, *46*, 855−874.
(12) Yang, N.; Cheng, H.; Liu, X.; Yun, Q.; Chen, Y.; Li, B.; Chen, B.; Zhang, Z.; Chen, X.; Lu, Q.; Huang, J.; Huang, Y.; Zong, Y.; Yang, Y.; Gu, L.; Zhang, H. Amorphous/Crystalline Hetero-Phase Pd Nanosheets: One-Pot Synthesis and Highly Selective Hydrogenation Reaction. *Adv. Mater.* **2018**, *30*, 1803234.
(13) Fan, Z.; Bosman, M.; Huang, X.; Huang, D.; Yu, Y.; Ong, K. P.; Akimov, Y. A.; Wu, L.; Li, B.; Wu, J.; Huang, Y.; Liu, Q.; Eng Png, C.; Lip Gan, C.; Yang, P.; Zhang, H. Stabilization of 4H hexagonal phase in gold nanoribbons. *Nat. Commun.* **2015**, *6*, 7684.
(14) Huang, X.; Li, S.; Huang, Y.; Wu, S.; Zhou, X.; Li, S.; Gan, C. L.; Boey, F.; Mirkin, C. A.; Zhang, H. Synthesis of hexagonal close-packed gold nanostructures. *Nat. Commun.* **2011**, *2*, 292.
(15) Jin, H.; Guo, C.; Liu, X.; Liu, J.; Vasileff, A.; Jiao, Y.; Zheng, Y.; Qiao, S.-Z. Emerging Two-Dimensional Nanomaterials for Electrocatalysis. *Chem. Rev.* **2018**, *118*, 6337−6408.
(16) Tang, K.; Zhang, J.; Yan, W.; Li, Z.; Wang, Y.; Yang, W.; Xie, Z.; Sun, T.; Fuchs, H. One-Step Controllable Synthesis for High-Quality Ultrafine Metal Oxide Semiconductor Nanocrystals via a Separated Two-Phase Hydrolysis Reaction. *J. Am. Chem. Soc.* **2008**, *130*, 2676−2680.
(17) Liu, L.; Wu, J.; Wu, L.; Ye, M.; Liu, X.; Wang, Q.; Hou, S.; Lu, P.; Sun, L.; Zheng, J.; Xing, L.; Gu, L.; Jiang, X.; Xie, L.; Jiao, L. Phase-selective synthesis of 1T′ MoS_2 monolayers and heterophase bilayers. *Nat. Mater.* **2018**, *17*, 1108−1114.
(18) Yu, Y.; Nam, G. H.; He, Q.; Wu, X. J.; Zhang, K.; Yang, Z.; Chen, J.; Ma, Q.; Zhao, M.; Liu, Z.; Ran, F. R.; Wang, X.; Li, H.; Huang, X.; Li, B.; Xiong, Q.; Zhang, Q.; Liu, Z.; Gu, L.; Du, Y.; Huang, W.; Zhang, H. High phase-purity 1T′-MoS_2- and 1T′-$MoSe_2$-layered crystals. *Nat. Chem.* **2018**, *10*, 638−643.
(19) Zhang, H.; Finnegan, M.; Banfield, J. F. Preparing Single-Phase Nanocrystalline Anatase from Amorphous Titania with Particle Sizes Tailored by Temperature. *Nano Lett.* **2001**, *1*, 81−85.
(20) Tan, C.; Cao, X.; Wu, X. J.; He, Q.; Yang, J.; Zhang, X.; Chen, J.; Zhao, W.; Han, S.; Nam, G. H.; Sindoro, M.; Zhang, H. Recent Advances in Ultrathin Two-Dimensional Nanomaterials. *Chem. Rev.* **2017**, *117*, 6225−6331.
(21) Zheng, Y.; Jiao, Y.; Vasileff, A.; Qiao, S.-Z. The Hydrogen Evolution Reaction in Alkaline Solution: From Theory, Single Crystal Models, to Practical Electrocatalysts. *Angew. Chem., Int. Ed.* **2018**, *57*, 7568−7579.
(22) Kang, Y.; Najmaei, S.; Liu, Z.; Bao, Y.; Wang, Y.; Zhu, X.; Halas, N. J.; Nordlander, P.; Ajayan, P. M.; Lou, J.; Fang, Z. Plasmonic hot electron induced structural phase transition in a MoS_2 monolayer. *Adv. Mater.* **2014**, *26*, 6467−6471.
(23) Li, H.; Chen, S.; Jia, X.; Xu, B.; Lin, H.; Yang, H.; Song, L.; Wang, X. Amorphous nickel-cobalt complexes hybridized with 1T-phase molybdenum disulfide via hydrazine-induced phase transformation for water splitting. *Nat. Commun.* **2017**, *8*, 15377.
(24) Liu, Q.; Li, X.; He, Q.; Khalil, A.; Liu, D.; Xiang, T.; Wu, X.; Song, L. Gram-Scale Aqueous Synthesis of Stable Few-Layered 1T-MoS_2: Applications for Visible-Light-Driven Photocatalytic Hydrogen Evolution. *Small* **2015**, *11*, 5556−5564.
(25) Enyashin, A. N.; Yadgarov, L.; Houben, L.; Popov, I.; Weidenbach, M.; Tenne, R.; Bar-Sadan, M.; Seifert, G. New Route for Stabilization of 1T-WS_2 and MoS_2 Phases. *J. Phys. Chem. C* **2011**, *115*, 24586−24591.
(26) Li, H.; Chen, S.; Zhang, Y.; Zhang, Q.; Jia, X.; Zhang, Q.; Gu, L.; Sun, X.; Song, L.; Wang, X. Systematic design of superaerophobic nanotube-array electrode comprised of transition-metal sulfides for overall water splitting. *Nat. Commun.* **2018**, *9*, 2452.
(27) Mahler, B.; Hoepfner, V.; Liao, K.; Ozin, G. A. Colloidal synthesis of 1T-WS_2 and 2H-WS_2 nanosheets: applications for photocatalytic hydrogen evolution. *J. Am. Chem. Soc.* **2014**, *136*, 14121−14127.
(28) Li, W.; Huang, H.; Li, H.; Zhang, W.; Liu, H. Facile synthesis of pure monoclinic and tetragonal zirconia nanoparticles and their phase effects on the behavior of supported molybdena catalysts for methanol-selective oxidation. *Langmuir* **2008**, *24*, 8358−8366.
(29) Yamaguchi, T.; Hightower, J. W. Hydrogenation of 1, 3-butadiene with 1, 3-cyclohexadiene and molecular deuterium over zirconium dioxide catalysts. *J. Am. Chem. Soc.* **1977**, *99*, 4201−4203.
(30) He, D.; Ding, Y.; Luo, H.; Li, C. Effects of zirconia phase on the synthesis of higher alcohols over zirconia and modified zirconia. *J. Mol. Catal. A: Chem.* **2004**, *208*, 267−271.
(31) Garvie, R. C. Stabilization of the tetragonal structure in zirconia microcrystals. *J. Phys. Chem.* **1978**, *82*, 218−224.
(32) Tang, J.; Zhang, F.; Zoogman, P.; Fabbri, J.; Chan, S. W.; Zhu, Y.; Brus, L. E.; Steigerwald, M. L. Martensitic Phase Transformation of Isolated HfO_2, ZrO_2, and $Hf_xZr_{1-x}O_2$ ($0 < x < 1$) Nanocrystals. *Adv. Funct. Mater.* **2005**, *15*, 1595−1602.
(33) Xu, X.; Wang, X. Fine tuning of the sizes and phases of ZrO_2 nanocrystals. *Nano Res.* **2009**, *2*, 891−902.
(34) Katoh, R.; Furube, A.; Yoshihara, T.; Hara, K.; Fujihashi, G.; Takano, S.; Murata, S.; Arakawa, H.; Tachiya, M. Efficiencies of electron injection from excited N3 dye into nanocrystalline semiconductor (ZrO_2, TiO_2, ZnO, Nb_2O_5, SnO_2, In_2O_3) films. *J. Phys. Chem. B* **2004**, *108*, 4818−4822.
(35) Zhang, D.; Liu, Z.; Li, C.; Tang, T.; Liu, X.; Han, S.; Lei, B.; Zhou, C. Detection of NO2 down to ppb levels using individual and multiple In_2O_3 nanowire devices. *Nano Lett.* **2004**, *4*, 1919−1924.
(36) Li, Z.; Xie, Z.; Zhang, Y.; Wu, L.; Wang, X.; Fu, X. Wide band gap p-block metal oxyhydroxide InOOH: a new durable photocatalyst for benzene degradation. *J. Phys. Chem. C* **2007**, *111*, 18348−18352.
(37) Chu, D.; Zeng, Y.-P.; Jiang, D.; Xu, J. Tuning the phase and morphology of In_2O_3 nanocrystals via simple solution routes. *Nanotechnology* **2007**, *18*, 435605.
(38) Xu, X.; Wang, X. Size-and surface-determined transformations: from ultrathin InOOH nanowires to uniform c-In_2O_3 Nanocubes and rh-In_2O_3 nanowires. *Inorg. Chem.* **2009**, *48*, 3890−3895.
(39) Hoffmann, M. R.; Martin, S. T.; Choi, W.; Bahnemann, D. W. Environmental applications of semiconductor photocatalysis. *Chem. Rev.* **1995**, *95*, 69−96.
(40) Wu, M.; Lin, G.; Chen, D.; Wang, G.; He, D.; Feng, S.; Xu, R. Sol-hydrothermal synthesis and hydrothermally structural evolution of nanocrystal titanium dioxide. *Chem. Mater.* **2002**, *14*, 1974−1980.
(41) Li, G.; Li, L.; Boerio-Goates, J.; Woodfield, B. F. High purity anatase TiO_2 nanocrystals: near room-temperature synthesis, grain growth kinetics, and surface hydration chemistry. *J. Am. Chem. Soc.* **2005**, *127*, 8659−8666.
(42) Xiang, G.; Wang, Y. G.; Wu, D.; Li, T.; He, J.; Li, J.; Wang, X. Size-dependent surface activity of rutile and anatase TiO_2 nanocrystals: facile surface modification and enhanced photocatalytic performance. *Chem. - Eur. J.* **2012**, *18*, 4759−4765.
(43) Jin, H.; Liu, X.; Vasileff, A.; Jiao, Y.; Zhao, Y.; Zheng, Y.; Qiao, S.-Z. Single-Crystal Nitrogen-Rich Two-Dimensional Mo5N6 Nanosheets for Efficient and Stable Seawater Splitting. *ACS Nano* **2018**, *12*, 12761−12769.
(44) Mitsuhashi, T.; Kleppa, O. J. Transformation enthalpies of the TiO_2 polymorphs. *J. Am. Ceram. Soc.* **1979**, *62*, 356−357.
(45) Mitsuhashi, T.; Ichihara, M.; Tatsuke, U. Characterization and stabilization of metastable tetragonal ZrO_2. *J. Am. Ceram. Soc.* **1974**, *57*, 97−101.
(46) Williamson, G. K.; Hall, W. H. X-ray line broadening from filed aluminium and wolfram. *Acta Metall.* **1953**, *1*, 22−31.
(47) Vargas, S.; Arroyo, R.; Haro, E.; Rodríguez, R. Effects of cationic dopants on the phase transition temperature of titania prepared by the sol-gel method. *J. Mater. Res.* **1999**, *14*, 3932−3937.

DOI: 10.1021/acs.accounts.8b00645
Acc. Chem. Res. 2019, 52, 780−790

(48) Chen, B.; Zhang, H.; Gilbert, B.; Banfield, J. F. Mechanism of inhibition of nanoparticle growth and phase transformation by surface impurities. *Phys. Rev. Lett.* **2007**, *98*, 106103.
(49) Zhuang, Z.; Peng, Q.; Li, Y. Controlled synthesis of semiconductor nanostructures in the liquid phase. *Chem. Soc. Rev.* **2011**, *40*, 5492−5513.
(50) Xiang, G.; Li, T.; Zhuang, J.; Wang, X. Large-scale synthesis of metastable TiO2(B) nanosheets with atomic thickness and their photocatalytic properties. *Chem. Commun.* **2010**, *46*, 6801−6803.
(51) Xiang, G.; Wang, Y.-G.; Li, J.; Zhuang, J.; Wang, X. Surface-specific interaction by structure-match confined pure high-energy facet of unstable TiO_2(B) polymorph. *Sci. Rep.* **2013**, *3*, 1411.
(52) Boles, M. A.; Ling, D.; Hyeon, T.; Talapin, D. V. The surface science of nanocrystals. *Nat. Mater.* **2016**, *15*, 141−153.
(53) Deng, D.; Novoselov, K. S.; Fu, Q.; Zheng, N.; Tian, Z.; Bao, X. Catalysis with two-dimensional materials and their heterostructures. *Nat. Nanotechnol.* **2016**, *11*, 218−230.
(54) Sun, Y.; Gao, S.; Lei, F.; Xie, Y. Atomically-thin two-dimensional sheets for understanding active sites in catalysis. *Chem. Soc. Rev.* **2015**, *44*, 623−636.
(55) Xiang, G.; Tang, Y.; Liu, Z.; Zhu, W.; Liu, H.; Wang, J.; Zhong, G.; Li, J.; Wang, X. Probing Ligand-Induced Cooperative Orbital Redistribution That Dominates Nanoscale Molecule−Surface Interactions with One-Unit-Thin TiO_2 Nanosheets. *Nano Lett.* **2018**, *18*, 7809−7815.
(56) Jamesh, M. I. Recent progress on earth abundant hydrogen evolution reaction and oxygen evolution reaction bifunctional electrocatalyst for overall water splitting in alkaline media. *J. Power Sources* **2016**, *333*, 213−236.
(57) Wu, Y.; Li, G.-D.; Liu, Y.; Yang, L.; Lian, X.; Asefa, T.; Zou, X. Overall Water Splitting Catalyzed Efficiently by an Ultrathin Nanosheet-Built, Hollow Ni_3S_2-Based Electrocatalyst. *Adv. Funct. Mater.* **2016**, *26*, 4839−4847.

DOI: 10.1021/acs.accounts.8b00645
Acc. Chem. Res. 2019, 52, 780−790